

# Coherent spinor dynamics in a spin-1 Bose condensate

Ming-Shien Chang, Qishu Qin, Wenxian Zhang, Li You, and Michael S. Chapman

*School of Physics, Georgia Institute of Technology,  
Atlanta, Georgia 30332-0430, USA*

(Dated: September 12, 2018)

Collisions in a thermal gas are perceived as random or incoherent as a consequence of the large numbers of initial and final quantum states accessible to the system. In a quantum gas, e.g. a Bose-Einstein condensate or a degenerate Fermi gas, the phase space accessible to low energy collisions is so restricted that collisions become coherent and reversible. Here, we report the observation of coherent spin-changing collisions in a gas of spin-1 bosons. Starting with condensates occupying two spin states, a condensate in the third spin state is coherently and reversibly created by atomic collisions. The observed dynamics are analogous to Josephson oscillations in weakly connected superconductors and represent a type of matter-wave four-wave mixing. The spin-dependent scattering length is determined from these oscillations to be  $-1.45(32)$  Bohr. Finally, we demonstrate coherent control of the evolution of the system by applying differential phase shifts to the spin states using magnetic fields.

PACS numbers:

Bose-Einstein condensation (BEC) is a well-known phenomenon in which identical bosons occupy the same quantum state below a certain critical temperature. A hallmark of BEC is the coherence between particles—every particle shares the same quantum wave function and phase. Although textbook discussions of Bose-Einstein condensation typically focus on non-interacting (ideal) particles, elastic collisions are essential in order for a quantum degenerate gas to equilibrate. The inclusion of collisions also modifies the quantum ground state of the gas, although it does not change the nature of the coherence of the condensate—indeed it has been pointed out that collisional interactions are in fact required to keep the condensate from fragmenting into multiple nearby quantum states [1].

Collisional coherence is an important theme in quantum degenerate gases. For single component condensates, such as spin-polarized atomic condensates confined in a magnetic trap, the coherence of the collisional interactions manifests through the coherence of the many-particle wave function itself, which has been well-established in early measurements of condensate mean-field energy [2] and correlations [3] as well as in demonstrations of matter-wave interference [4] and superfluid behaviour [5, 6, 7]. More recently, collisional coherence in more complicated systems has led to remarkable demonstrations including reversible atom-molecule formation across a Feshbach resonance for both bosonic and fermionic [8, 9] atoms, and coherent collisions in optical lattices [10, 11].

In this work, we show that the collisional coherence extends to the internal spin degrees of freedom of a spin-1 Bose gas by observing coherent and reversible spin-changing collisions. Atomic Bose condensates with internal spin, so-called spinor condensates [12, 13, 14, 15, 16, 17, 18, 19, 20], in some cases, are predicted to coherently inter-convert in a process known

as spin mixing, driven solely by internal interactions in the system [21, 22, 23, 24, 25, 26]. In a spin-1 condensate, two atoms with spin components  $-1$  and  $+1$  can coherently and reversibly scatter into final states containing two atoms with spin component  $0$  and vice-versa (Fig. 1a). We observe this process in a gas of spin-1  $^{87}\text{Rb}$  bosons confined in an all-optical trap. The coherent spin mixing leads to oscillations of the spin populations, from which we determine the spin-dependent interaction strength. This is the first direct measurement of this important quantity. The observed spin-mixing is an internal state analogue to Josephson oscillations in weakly connected superconductors [27], and exploiting this analogy, we demonstrate control of the coherent spinor dynamics using phase and population engineering. Finally, we use this technique to drive the spinor condensate to and away from its spin ground state, which allows us to measure the spin coherence time [21].

Stimulated by the seminal theoretical work by Ho [12] and Ohmi and Machida [13] and early experiments by the JILA [14, 28] and MIT [15] groups, much study has been done on spinor condensates. Theoretical work has covered ground state structure [12, 13, 20, 21, 29], coherent spinor dynamics [21, 22, 23, 24, 25, 26], rotating spinor condensates [30] and many other topics. Spin mixing has been observed in both  $F = 1$  and  $F = 2$  condensates [15, 18, 19, 31], although the coherence of this process has not yet been demonstrated conclusively. Observations thus far have revealed mostly incoherent relaxation of initially non-equilibrium spin populations to lower energy configurations from which the sign of the spin interaction parameter  $c_2$  was determined. Although overdamped single oscillations in spin populations have been observed in earlier experiments by us and others, their interpretation has been limited because the initial spin configurations in these experiments were metastable, and evolution from these states is noise-driven [15, 18, 19, 31].

Nonetheless, from these observations, as well as studies of spin domain formation, it was possible to determine the magnetic nature of the ground states.

At the microscopic level, the interactions in spinor Bose gases are determined by spin-dependent 2-body collisions. In the case of two colliding spin- $F$  identical bosons, the available collision channels are restricted by symmetry to those with total spin  $F_{tot} = 2F, 2F - 2, \dots, 0$ , characterized by s-wave scattering lengths  $a_{F_{tot}}$  at low energies. We focus on the  $F = 1$  case here, and in the framework of mean-field theory, the interaction energy including spin can be written as  $U(r) = \delta(r)(c_0 + c_2 \vec{F}_a \cdot \vec{F}_b)$ , [12, 13] where  $r$  is the distance between two atoms  $a, b$  and  $c_0 = 4\pi\hbar^2(a_0 + 2a_2)/3m$  and  $c_2 = 4\pi\hbar^2(a_2 - a_0)/3m$ , where  $m$  is the atomic mass and  $a_{0,2}$  are the s-wave scattering lengths for total spin 0,2 channels. For  $^{87}\text{Rb}$  atoms in the  $F = 1$  hyperfine state, the scattering lengths the  $a_{0,2}$  are nearly equal, and hence the spin-dependent mean field energy  $c_2 n$  is very small (only 200 pK [32, 33] for typical densities,  $n \sim 10^{14} \text{ cm}^{-3}$ ), compared to both the scalar mean field  $c_0 n$ , and the estimated temperature of the gas, 50 nK. Nonetheless, the small spin-dependent mean field couplings are non-negligible and lead to qualitatively different ground state structures depending on the sign of  $c_2$ , being ferromagnetic ( $c_2 < 0$ ) for  $^{87}\text{Rb}$  [18, 19, 32, 33] or anti-ferromagnetic ( $c_2 > 0$ ) for  $^{23}\text{Na}$  [15, 34]. Moreover, these spinor interactions yield a rich variety of coherent and incoherent phenomena including coherent spinor mixing, spin squeezing and entanglement [21, 35], spin domain formation, and spinor vortices.

A single-component (scalar) atomic condensate with a large number of atoms is well-described within a mean-field treatment by an order parameter ('condensate wave function') governed by nonlinear Schrödinger or Gross-Pitaevskii (G-P) equation. For an  $F = 1$  spinor condensate, the three spin components  $m_F = 1, 0, -1$  are described by a vector order parameter,  $\vec{\psi}(\vec{r}, t) = (\psi_1, \psi_0, \psi_{-1})$  which is governed by a set of three coupled G-P equations [12, 21]

$$i\hbar \frac{\partial \psi_1}{\partial t} = L_1 \psi_1 + c_2(n_0 + n_1 - n_{-1})\psi_1 + c_2 \psi_{-1}^* \psi_0^2 \quad (1)$$

$$i\hbar \frac{\partial \psi_0}{\partial t} = L_0 \psi_0 + c_2(n_1 + n_{-1})\psi_0 + 2c_2 \psi_0^* \psi_1 \psi_{-1} \quad (2)$$

$$i\hbar \frac{\partial \psi_{-1}}{\partial t} = L_{-1} \psi_{-1} + c_2(n_0 + n_{-1} - n_1)\psi_{-1} + c_2 \psi_{+1}^* \psi_0^2 \quad (3)$$

where  $L_{\pm 1,0} = (-\hbar^2 \nabla^2 / 2m + V_t + E_{\pm 1,0} + c_0 n - \mu)$ ,  $V_t$ ,  $E_{\pm 1,0}$  and  $n_{\pm 1,0}$  are the optical trapping potential, Zeeman energies and densities for corresponding Zeeman projections,  $\mu$  is the chemical potential, and  $n = n_1 + n_0 + n_{-1}$  is the total density. The coherent spin mixing of the internal populations responsible for oscillations of the spin populations are determined

by the last term in Eqs.1-3. However, the interplay of this process with the particle exchange collisions, represented by the penultimate term in Eqs. 1-3 poses challenging problems both in theory and in experiment because they occur with the same time scale (typically  $< 10$  Hz for  $^{87}\text{Rb}$ ), and they are both very sensitive to external magnetic fields and field gradients represented in  $E_{\pm 1,0}$  [15, 18, 20, 26, 31, 36, 37]. Hence, in general, the dynamics described by these equations reveal a rich coupling between the internal and external degrees of freedom of the condensate components resulting in a variety of observed phenomena including spin mixing [15, 18, 19], spin domain formation [15], and spin textures [30, 38].

Although the internal and external dynamics are generally inseparable, under certain conditions they can be decoupled. In particular, when the available spin interaction energy is insufficient to create spatial spin structures in the condensates, then the external dynamics will be suppressed. This occurs when the spin healing length  $\xi_s = \hbar / \sqrt{2m |c_2| n}$  is larger than the size of the condensate. In this case, then  $\psi_1$ ,  $\psi_0$  and  $\psi_{-1}$  share the same spatial wave function  $\sqrt{n(\vec{r})} e^{-i\mu t / \hbar}$  which allows for a considerable simplification of Eq. 1-3. This is known as the single mode approximation (SMA), with which the order parameter reduces to  $\sqrt{n(\vec{r})} e^{-i\mu t / \hbar} \vec{\chi}$ , where  $\vec{\chi}^T = (\sqrt{\rho_1} e^{i\phi_1}, \sqrt{\rho_0} e^{i\phi_0}, \sqrt{\rho_{-1}} e^{i\phi_{-1}})$  and  $\rho_i$  and  $\phi_i$  represent the fractional population and phase of the  $i^{\text{th}}$  Zeeman state. With this approximation, the internal dynamics take on a particularly simple form determined by just two dynamical variables,  $\rho_0(t)$ , the fractional population of the 0 state, and the relative phase of the spinor components  $\phi(t) \equiv \phi_1 + \phi_{-1} - 2\phi_0$  [23]. The populations of the other states are directly determined by  $\rho_{\pm 1} = (1 - \rho_0 \pm M)/2$ , where  $M = (N_1 - N_{-1})/N$  is the global magnetism which is a constant of the motion, and  $N_i$  is the number of atoms in the  $i^{\text{th}}$  Zeeman projection with  $N = N_1 + N_0 + N_{-1}$ . The energy (Hamiltonian) of the system in a uniform magnetic field then takes the following simple form [25, 26]:

$$E = c\rho_0[(1 - \rho_0 + \sqrt{(1 - \rho_0)^2 - M^2 \cos \phi})] + \delta(1 - \rho_0), \quad (4)$$

where  $c = c_2 N \int |\psi(r)|^4 dr$  is the effective spin-mixing rate, and  $\delta = (E_1 + E_{-1} - 2E_0)/2 \simeq 2\pi\hbar \cdot (72B^2 \text{ Hz})$  is the difference in energies of the magnetic Zeeman levels in a field of  $B$  gauss. Within the SMA, the ground state spin populations and relative phase are readily found for arbitrary magnetization and magnetic field by minimizing Eq. 4. In particular, for  $c(c_2) < 0$ , the energy of the system is minimized at low fields for relative phases  $\phi = 0$  and population  $\rho_0 = (1 - M^2)/2$  [23, 26]. For other non-equilibrium populations or phases, the system will have excess spin energy that can drive a coherent evolution of the spinor system.

The evolution of the system will follow Hamiltonian

equations of motion derived from Eq. 4 [26]:

$$\dot{\rho}_0 = \frac{2c}{\hbar} \rho_0 \sqrt{(1 - \rho_0)^2 - M^2} \sin \phi \quad (5)$$

$$\dot{\phi} = -\frac{2\delta}{\hbar} + \frac{2c}{\hbar} (1 - 2\rho_0) + \frac{2c(1 - \rho_0)(1 - 2\rho_0) - M^2}{\hbar \sqrt{(1 - \rho_0)^2 - M^2}} \cos \phi. \quad (6)$$

These coupled equations are nonlinear Josephson-type equations and point to the equivalency of spin mixing in a spin-1 condensate to Josephson systems realized in superconductors [27] and other superfluids [11, 14, 39, 40, 41, 42, 43, 44]. The non-linearity of these equations provides a rich manifold of dynamical trajectories that can be accessed experimentally by choice of initial populations and phases of the spin components and the strength of the applied magnetic field.

To investigate the coherent dynamics of this system, we begin with  $^{87}\text{Rb}$  condensates created using an improved version of the all-optical trapping technique we have previously reported [16, 19]. Using a dynamical compression technique and just a single focused laser beam, condensates with up to 300,000 atoms are created after 2 s of evaporative cooling. The condensates created in this optical trap are generally in a mixture of all  $F = 1$  spin states and reveal complicated spatial domains. To create a well-characterized initial condition, we first prepare a condensate in the  $|F = 1, m_F = -1\rangle$  state by applying a magnetic field gradient during the evaporative cooling.

To initiate spin dynamics, a coherent superposition of spin states with non-equilibrium spin populations is created by applying a sequence of phase-coherent microwave pulses tuned to  $F = 1 \leftrightarrow F = 2$  transitions. Following this state preparation, the condensate is allowed to freely evolve in the optical trap. A typical evolution is shown in Fig. 1c for an initial spin configuration of  $\rho_{(1,0,-1)} \simeq (0, 3/4, 1/4)$ . Up to four distinct oscillations are observed in this example before the spin populations damp to a steady state. These oscillations demonstrate the coherence of the spin mixing process.

We have measured the spin oscillation frequency for different initial spin populations. These data are shown in the inset of Fig. 1c. and show good agreement with theoretical predictions,  $c\sqrt{1 - \rho_0^2}$  [23, 26] which can be derived from Eq. 5-6. These measurements provide a direct determination of the magnitude of the spin interaction energy [21],  $|c|/\hbar = 2\pi \times 4.3(3)$  rad/s for our system. These oscillation frequencies at low magnetic field do not determine the sign of  $c(c_2)$ , however it was established by previous studies of the nature of the ground state (and confirmed in the present study by the results shown later in Fig. 3) that  $c_2 < 0$  for the  $F = 1$  manifold of  $^{87}\text{Rb}$ . This value of  $c$ , combined with the measured condensate density,  $n = 2.1(4) \times 10^{14} \text{ cm}^{-3}$ , determined from the rate of the condensate expansion during time-of-flight, permits determination of  $c_2$ , or equivalently, the difference

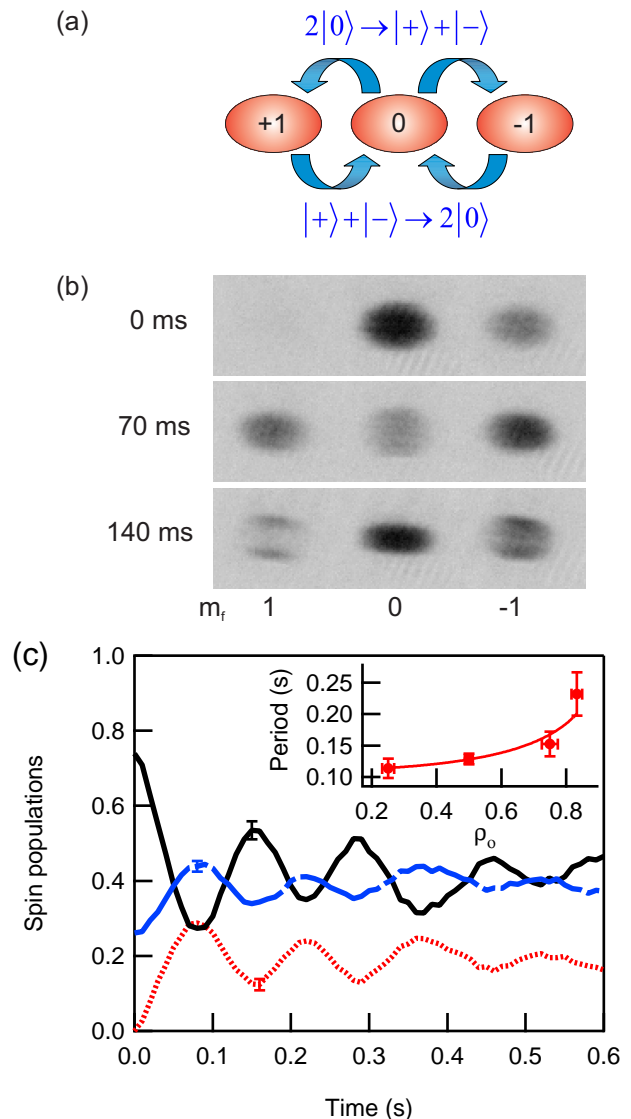


FIG. 1: Coherent spin mixing of spin-1 Bose condensate in an optical trap. Coherent spin mixing producing oscillations in the populations of the  $F = 1$ ,  $m_F = 0, \pm 1$  spin states of  $^{87}\text{Rb}$  condensates confined in an optical trap starting from a superposition of condensate spin components at  $t = 0$  that is subsequently allowed to evolve freely. a) Schematic indicates fundamental spin mixing process. b) Absorptive images of the condensates for different evolution times. In this example, the initial relative populations are  $\rho_{(1,0,-1)} \simeq (0, 3/4, 1/4)$ . The condensates are probed 18 ms after release from the trap, and, to separate the spin components for imaging, a weak magnetic field gradient is applied for 3 ms during expansion of the condensates. The field of view is  $600 \mu\text{m} \times 180 \mu\text{m}$ . c) Spin populations vs. evolution time for the same initial population configuration showing four clear oscillations. The damping of the oscillations is due to the breakdown of the single mode approximation readily apparent in the  $t = 140$  ms absorptive image. Here the dotted, solid, and dot-dashed lines represent the populations in  $m_F = 1, 0$  and  $-1$  states. Inset shows the measured oscillation period versus the initial population of the 0 state for different initial superpositions of  $m_F = 0, -1$  states, which compares well with the theoretical prediction [23]. The (typical) error bars shown are the standard deviation of three repeated measurements.

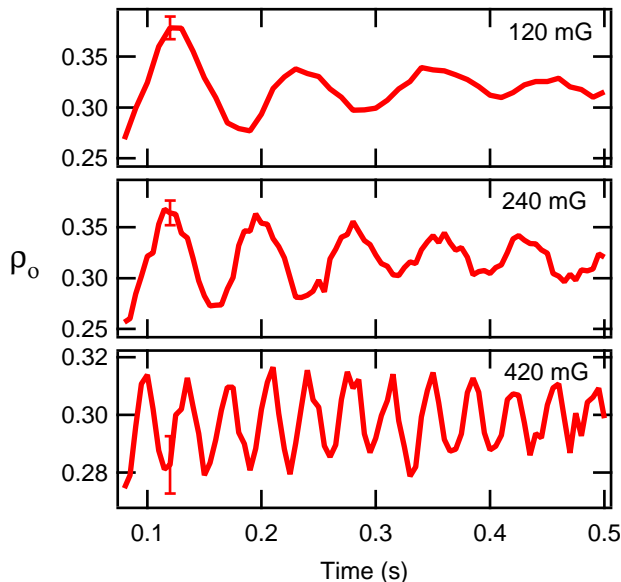


FIG. 2: Coherent spin mixing vs. magnetic field. An initial non-equilibrium spin population configuration of  $\rho_{(1,0,-1)} \simeq (0, 1/2, 1/2)$  is created and allowed to evolve in a field of 15 mG for 70 ms to allow for maximum spin mixing. At this point, the magnetic field is ramped to different levels. Subsequently, the system displays small amplitude oscillations analogous to the AC Josephson effect,  $\rho_0(t) \propto \delta^{-1} \sin 2\delta t$ . The typical error bars shown are the standard deviation of three repeated measurements.

in scattering lengths  $a_2 - a_0 = -1.45(32)a_B$ , where Bohr radius  $a_B = 0.529 \text{ \AA}$ . This is the first direct measurement of this important quantity, and our value agrees with the theoretical determination of  $a_2 - a_0 = -1.40(22)a_B$  derived from photoassociative spectroscopic and Feshbach resonance data [32, 33].

The oscillations are observed to damp with a time constant of 250 ms, and the damping coincides with the appearance of spatial spin structures apparent in the images in Fig. 1b. These structures indicate the invalidation of the SMA underlying Eqs. 5-6 and lead to a complicated interplay of the internal and external dynamics that ultimately transfers the internal spin energy into spatial domain structures [23]. A detailed study of these structures will be the focus of future work.

The large amplitude oscillations observed in Fig. 1c are in the nonlinear regime of Eqs 5-6. It is also possible to access the linear regime more typical of the standard Josephson effect by tuning the parameters of the system. In particular, for large applied magnetic fields such that  $\delta \gg c$  and appropriate initial populations, the phase evolution is dominated by the quadratic Zeeman effect of the external field, and Eq. 6 reduces to  $\dot{\phi} \simeq -2\delta/\hbar$ . For these conditions, the system exhibits small oscillations analogous to AC-Josephson oscillations,  $\rho_0(t) \simeq A\delta^{-1} \sin 2\delta t$ , where  $A$  is determined by the initial populations. We

have observed these oscillations as shown in Fig. 2. for different applied magnetic fields. Up to 12 fast oscillations are observed at the highest fields that were studied, where the time scale of the internal spinor dynamics is better separated from the time scale for the formation of spatial spin structures. The frequency of the measured oscillations vs. the magnetic field matches within 10% of the prediction  $\Omega = 2\delta$ , while the  $\delta^{-1}$  scaling for the amplitude is seen only for higher fields, presumably due to the invalidity of the SMA for larger amplitude oscillations. In the future, being able to tune the system to the linear regime provides a path to study many analogous effects previously observed in Josephson systems such as Shapiro levels [27, 36, 41, 45] by including a time-varying component to the applied magnetic field.

Beyond controlling the system via the initial conditions, the dynamical evolution of the system can be controlled in real time by either changing spin populations and/or changing the spinor phase  $\phi$ . We demonstrate that we can coherently control the dynamical evolution of the spinor by applying phase shifts, and in particular we drive the systems to the ferromagnetic spinor ground state using this technique. In this experiment, an initial non-equilibrium spin configuration is created and allowed to evolve for a fraction of an oscillation until  $\rho_0(t)$  reaches the ground-state ratio  $\rho_{0,gs} = (1 - M^2)/2$  [23, 29]. At this point, the system is not in the ground state because  $\phi \neq (\phi_{gs} = 0)$  (and it is still oscillating!) At this moment, we briefly pulse on a magnetic field of 0.6 G to apply a phase shift to the spinor,  $\Delta\phi = \int \delta(t)dt$ . The evolution of the system is recorded in Fig. 3a for different pulse durations. We find that for particular applied phase shifts, the spinor condensate is brought to its ground state, evidenced by the subsequent lack of population oscillation. For other applied phase shifts, the system is driven to different points in the phase space of the system, for which the subsequent evolution of the system is dramatically different and exhibits oscillations.

It is possible to reconstruct the dynamical trajectories of the system using the measured  $\rho_0(t)$ , along with the known applied phase shifts and the equations of motion, Eqs. 5-6. Although the damping evident in the measurement is due to the spatial dynamics coupled to the internal spin mixing dynamics, a phenomenological phase damping term may be added to Eq. 6 to represent the spatial varying spin mixing rate which is responsible for damping the population oscillation. The reconstructed trajectories show good qualitative agreement with the measurements in the time domain and are plotted on the phase space diagram of the system (Fig. 3b). Also shown in the figure are the contours of equal energy of the spinor given by Eq. 4. The trajectories clearly show that the system tends to damp to the minimum energy points (i.e. the ferromagnetic spinor ground state), which is  $\rho_0 \simeq 3/8$ ,  $\phi_{gs} = 0 \pmod{2\pi}$  for  $M = 1/2$ ,  $c < 0$  and  $\delta \approx 0$ . For the case of anti-ferromagnetic interac-

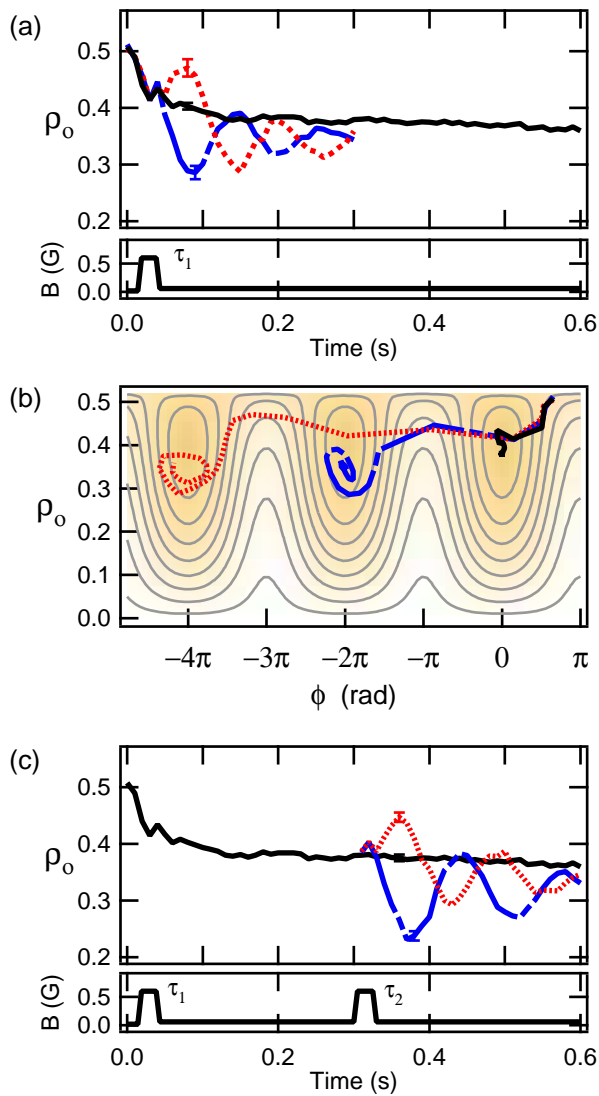


FIG. 3: Coherent control of spinor dynamics. a) An initial spin configuration of  $\rho_{(1,0,-1)} \simeq (0, 1/2, 1/2)$  is allowed to evolve in a field of 15 mG for 14 ms at which point the populations reach the values corresponding to the ferromagnetic ground state at this magnetization:  $\rho_{(1,0,-1)} \simeq (1/16, 3/8, 9/16)$ . Then, a pulse of 600 mG field is applied to shift the spinor phase. The dashed, solid and dotted curves represent pulse widths of  $\tau_1 = 20, 24.4$  and 30 ms respectively. For certain applied phase shifts, the coherent spin mixing can be halted. This occurs for  $\tau_1 = 24.4$  ms corresponding to phase shift  $\Delta\phi = -2.5\pi$  and for  $\tau_1 = 5.3$  ms corresponding to  $\Delta\phi = -0.5\pi$ . b) Reconstructed dynamical trajectories of the system determined by fitting the experiment data to Eq. 3,4 including a phenomenological phase damping term. The free parameters of the fit are the damping coefficient and the unknown (but reproducible) initial spinor phase resulting from the state preparation that depends on the applied microwave pulse width and the duration in the upper hyperfine manifold. The contours show curves of equal energy. c) To investigate the spin coherence of the ground state spinor created by the first pulse with  $\tau_1 = 24.4$  ms, a second pulse is applied at 300 ms to reestablish the oscillations. The solid, dashed and dotted curves corresponds to  $\tau_2 = 0, 10$  and 20 ms respectively. The typical error bars shown are the standard deviation of three repeated measurements.

tions, such as in  $^{23}\text{Na}$ ,  $c > 0$ , the energy contours differ only in sign, and the system would instead relax to  $\rho_0 = 1$ ,  $\phi_{gs} = \pi \pmod{2\pi}$  within the validity of the SMA [23, 29].

To demonstrate explicitly the coherence of the spinor ground state, we impart a second phase shift to the system at later times to displace the system to a different point in phase space. As anticipated, the second phase shift is found to re-initiate the spin mixing dynamics (Fig. 3c) when  $\Delta\phi \neq 0 \pmod{2\pi}$ . We have used this technique to determine the ground state spinor decoherence time by measuring the amplitude of the subsequent oscillations for different delay times of the second pulse. The spinor decoherence time is found to be 3 s, which is approximately the lifetime of the condensate and is much longer than the damping time of spin population oscillations.

As noted, the damping of the spin oscillations coincides with the appearance of spin wave-like spatial structures in the spinor wave function (see images in Fig. 1b). Hence it is clear that the SMA is not strictly valid for our system. These waves derive their energy from the internal (spin) degrees of freedom, and it is this energy transfer that ultimately damps the spin mixing. On the other hand, if the spinor condensate is driven to its ferromagnetic ground state, as shown in Fig. 3b, there is no internal (spin) energy available for the motional degrees of freedom, and spatial spin structures cannot form. Indeed in this case, the three spin components are observed to have the same spatial wave function and appear to be miscible.

The observation of coherent spinor dynamics in a ferromagnetic spin-1 system reported here paves the way for a host of future explorations. These systems are predicted to manifest complex quantum correlated states exhibiting entanglement and squeezing, and in general, it will be very interesting to explore the regime of small atom number  $< 1000$ , where sub-shot noise effects should become important [21]. Viewing the spin-mixing dynamics as a type of internal Josephson effect, many future explorations and manipulations of the system can be envisaged following along the path of superconducting weak-links. Finally, the coupling of the internal dynamics to the spatial wave function can be avoided in future experiments by either decreasing the condensate radii relative to the spin healing length  $\xi_s$  and/or operating at high magnetic fields where the time scales for mixing and damping are better separated. On the other hand, the coupling of the internal and external degrees of freedom in this system provide a new system for exploring nonlinear atom optical phenomena such as spatial-temporal dynamics of four-wave mixing [46].

We note that a group in Mainz, Germany has independently observed coherent spin-mixing oscillations in a Mott state of atoms on a lattice [47]. Their experiment involves a system of many copies of two atoms in each

lattice site. On the other hand, our system involves a few hundred thousand atoms and the observed coherence reflects the presence of macroscopic quantum fields.

### Methods

To create the condensates, we begin by collecting up to  $5 \times 10^8$  cold atoms in a simple vapour cell  $^{87}\text{Rb}$  magneto-optical trap (MOT), which is overlapped with an optical trap formed by a single  $\text{CO}_2$  laser beam of 70 W focused to a waist of  $60 \mu\text{m}$ . Up to  $3.7 \times 10^7$  atoms are loaded into the optical trap, at a density of  $4 \times 10^{13} \text{ cm}^{-3}$ . In order to achieve higher densities for efficient evaporation, the trap is compressed immediately after loading by smoothly changing the laser focus to  $26 \mu\text{m}$  over 600 ms using a zoom lens. Simultaneously, the laser power is ramped down over 1.8 s to lower the trap depth and force evaporative cooling. Using this technique, mostly pure condensates containing up to  $3 \times 10^5$  atoms are created. This technique is not only simple and fast, but also produces condensates 10 times larger than our previous methods [16, 19]. The condensates created in this optical trap are generally in a mixture of all  $F = 1$  spin states and reveal complicated spatial domains. To create a well-characterized initial condition, we apply a magnetic field gradient during the evaporative cooling [19], which results in pure  $m_F = -1$  condensate containing 150,000 atoms—this state is stable against both local and global spin dynamics due to the conservation of angular momentum. The trap frequencies are  $2\pi(190,170,17)$  rad/s, and the condensate density and the Thomas-Fermi (T-F) radii are estimated to be  $2.1 \times 10^{14} \text{ cm}^{-3}$  and  $(3.2, 3.6, 36) \mu\text{m}$  respectively. The lifetime of the condensate is measured to be 3 s. Coherent spin state superpositions are created from the pure  $m_F = -1$  condensates by applying a sequence of phase-coherent microwave pulses tuned to  $F = 1 \leftrightarrow F = 2$  transitions. The pulses are applied at a field of 420 mG to separate out the transitions between the different Zeeman sub-levels. Following the pulse sequence, the magnetic field is ramped from 420 mG to 15 mG in 10 ms. Typical pulse lengths are 20 s for a  $F = 1 \leftrightarrow F = 2$  pulse.

**Acknowledgements.** This work was supported by nsf-physics 0303013 and NASA-NAG3-2893. We would like to thank C. Hamley, K. Fortier, J. Sauer and other members of the Georgia Tech Atomic Physics and Quantum Optics Group for their assistance, and H. Pu for valuable discussions.

- [2] J. R. Ensher, et al., Phys. Rev. Lett. **77**, 4984 (1996).
- [3] E. A. Burt, et al., Phys. Rev. Lett. **79**, 337 (1997).
- [4] M. R. Andrews, et al., Science **275**, 637 (1997).
- [5] K. W. Madison, et al., Phys. Rev. Lett. **84**, 806 (2000).
- [6] M. R. Matthews, et al., Phys. Rev. Lett. **83**, 2498 (1999).
- [7] J. R. Abo-Shaeer, et al., Science **292**, 476 (2001).
- [8] E. A. Donley, et al., Nature **417**, 529 (2002).
- [9] M. Greiner, et al., Nature **426**, 537 (2003).
- [10] M. Greiner, et al., Nature **415**, 39 (2002).
- [11] B. P. Anderson and M. A. Kasevich, Science **282**, 1686 (1998).
- [12] T. L. Ho, Phys. Rev. Lett. **81**, 742 (1998).
- [13] T. Ohmi and K. Machida, J. Phys. Soc. Jpn. **67**, 1822 (1998).
- [14] D. S. Hall, et al., Phys. Rev. Lett. **81**, 1543 (1998).
- [15] J. Stenger, et al., Nature **396**, 345 (1998).
- [16] M. D. Barrett, et al., Phys. Rev. Lett. **87**, 010404 (2001).
- [17] A. Gorlitz, et al., Phys. Rev. Lett. **90**, 090401 (2003).
- [18] H. Schmaljohann, et al., Phys. Rev. Lett. **92**, 040402 (2004).
- [19] M.-S. Chang, et al., Phys. Rev. Lett. **92**, 140403 (2004).
- [20] M. Koashi and M. Ueda, Phys. Rev. Lett. **84**, 1066 (2000).
- [21] C. K. Law, et al., Phys. Rev. Lett. **81**, 5257 (1998).
- [22] E. V. Goldstein and P. Meystre, Phys. Rev. A **59**, 3896 (1999).
- [23] H. Pu, et al., Phys. Rev. A **60**, 1463 (1999).
- [24] J. P. Burke, et al., Phys. Rev. A **70**, 033606 (2004).
- [25] D. R. Romano and E. J. V. de Passos, Phys. Rev. A **70**, 043614 (2004).
- [26] W. Zhang, et al., Phys. Rev. A **72**, 013602 (2005).
- [27] A. Barone and G. Paterno, Physics and applications of the Josephson effect (Wiley, New York, 1982).
- [28] D. S. Hall, et al., Phys. Rev. Lett. **81**, 1539-1542 (1998).
- [29] W. X. Zhang, et al., New J. Phys. **5**, 77 (2003).
- [30] A. E. Leanhardt, et al., Phys. Rev. Lett. **90**, 140403 (2003).
- [31] T. Kuwamoto, et al., Phys. Rev. A **69**, 063604 (2004).
- [32] N. N. Klausen, et al., Phys. Rev. A **64**, 053602 (2001).
- [33] E. G. M. van Kempen, et al., Phys. Rev. Lett. **88**, 093201 (2002).
- [34] J. P. Burke, et al., Phys. Rev. Lett. **81**, 3355 (1998).
- [35] L. M. Duan, et al., Phys. Rev. A **65**, 033619 (2002).
- [36] H. Pu, et al., Phys. Rev. A **61**, 023602 (2000).
- [37] H. J. Miesner, et al., Phys. Rev. Lett. **82**, 2228 (1999).
- [38] M. R. Matthews, et al., Phys. Rev. Lett. **83**, 3358 (1999).
- [39] A. J. Leggett, Rev. Mod. Phys. **47**, 331 (1975).
- [40] J. C. Wheatley, Rev. Mod. Phys. **47**, 415 (1975).
- [41] J. C. Davis and R. E. Packard, Rev. Mod. Phys. **74**, 741 (2001).
- [42] J. Javanainen, Phys. Rev. Lett. **57**, 3164 (1986).
- [43] A. Smerzi, et al., Phys. Rev. Lett. **79**, 4950 (1997).
- [44] F. S. Cataliotti, et al., Science **293**, 843 (2001).
- [45] S. Shapiro, Phys. Rev. Lett. **11**, 80 (1963).
- [46] L. Deng, et al., Nature **398**, 218 (1999).
- [47] A. Widera, et al., cond-mat/0505492 (2005).

---

[1] P. Nozières and D. S. James, J. Phys. (Paris) **43**, 1133 (1982).